

Experimental demonstration of ultrafast wavepacket containing orbital angular momentum with controllable orientation

CHENHAO WAN,^{1,2} JIAN CHEN,¹ ANDY CHONG,^{3,4} AND QIWEN ZHAN^{1,*}

¹ School of Optical-Electrical and Computer Engineering, University of Shanghai for Science and Technology, Shanghai 200093, China

² School of Optical and Electronic Information, Huazhong University of Science and Technology, Wuhan, Hubei 430074, China

³ Department of Electro-Optics and Photonics, University of Dayton, 300 College Park, Dayton, Ohio 45469, USA

⁴ Department of Physics, University of Dayton, 300 College Park, Dayton, Ohio 45469, USA

*qwzhan@usst.edu.cn

An optical vortex, generally associated with a spiral phase, can carry longitudinal orbital angular momentum (OAM) in the direction of beam propagation, or transverse OAM perpendicular to beam propagation. In this work, we introduce complex temporal and spatial features to optical OAM through stable collision of spatiotemporal and spatial vortices within one wave packet. Interactions between the transverse OAM carried by the spatiotemporal vortex and the longitudinal OAM carried by the spatial vortex are experimentally observed, showing a controllable orientation of the total OAM with respect to the propagation direction. Wavepacket containing rapidly varying OAM orientation is also demonstrated. The three-dimensional orientation and non-static temporal features empower novel applications of the OAM of photons.

1. Introduction

Vortices, ubiquitous in nature, are circulating disturbances of liquid, gas or other media. They have been found in turbulent water, circulating air around wingtips, swirling galaxies and optics as well [1]. Optical vortices are generally associated with a spiral phase in the cross section of a beam, i.e., x - y plane. The twisted phase gives rise to an azimuthally circulating component of Poynting vector that contributes to an integrated longitudinal orbital angular momentum (OAM) parallel with the beam axis [2-5]. Each photon carries an OAM of $l\hbar$ where \hbar is the reduced Planck's constant and l is an integer, generally referred to as the topological charge. The connection of vortex beams with longitudinal OAM has spurred substantial theoretical and experimental research and found a wealth of applications in both classical and quantum optics [6-10].

Not until very recently did scientists demonstrate that a spiral phase can also exist in the spatiotemporal domain, e.g., x - t plane [11,12]. The spiral phase is initially constructed in the spatial frequency - temporal frequency plane and then retained in the spatiotemporal plane after a two-dimensional Fourier transform. An ultrafast wave packet carrying a spatiotemporal vortex resembles a fast-moving cyclone, leading to peculiar transverse OAM in the direction perpendicular to beam propagation. The transverse OAM is intrinsic and determined by the topological charge of the spatiotemporal vortex.

A question naturally arises: Is it possible to obtain a three-dimensionally oriented OAM? An intuitive idea suggests that a three-dimensionally oriented OAM should be related to an optical vortex with a three-dimensionally oriented vortex line. In fact, theoretical explorations reveal that a tilted OAM can be obtained via Lorentz transformations of the usual spatial vortex, i.e., via fast-moving sources emitting spatial vortices in their rest frames [13]. However, it is nonintuitive to build a spiral phase with a tilted vortex line in a laboratory.

In this work, we theoretically and experimentally demonstrate that the average OAM per photon of a wave packet can be made three-dimensionally oriented through embedding stable collision of spatiotemporal vortices and spatial vortices within one wave packet. Both the orientation and the OAM value can be accurately controlled via the topological charges of spatiotemporal and spatial vortices. More importantly, we discover that it is even possible to embed multiple collisions of these orthogonal vortices resulting in a temporally non-static feature of OAM. Time-varying OAM has just been demonstrated through high-harmonic generation based on longitudinal OAM and has potential applications in imaging magnetic and topological excitations, manipulating the OAM dichroism of nanostructures, or selectively exciting chiral quantum matter [14]. Our work takes advantage of both transverse and longitudinal OAM and achieves time-varying and three-dimensionally oriented OAM. The complexity of both spatial and temporal features of optical OAM introduced in the current paper enriches the understanding of photonic torque and providing extraordinary tools for exploiting the power of the OAM of photons.

2. Theory

A wave packet is assumed to propagate in the z direction with a vector potential \mathbf{A} polarized in the x direction:

$$\mathbf{A} = u(x, y, z') e^{ikz'} \mathbf{x}, \quad (1)$$

where \mathbf{x} is the unit vector in the x direction, z is the propagation direction, z' is the local frame coordinate given by $z' = z - ct$, c is the speed of light in vacuum, and k is the wave number. $u(x, y, z')$ is a complex scalar function describing the field distribution under paraxial approximation. A spatiotemporal vortex of topological charge l_1 and a spatial vortex of topological charge l_2 are both embedded within the wave packet. The complex scalar function u is therefore given by,

$$u(x, y, z') = \left(\frac{x \pm i \operatorname{sgn}(l_1) y}{w_x} \right)^{|l_1|} \left(\frac{x \pm i \operatorname{sgn}(l_2) z'}{w_x} \right)^{|l_2|} \exp \left\{ - \left[\left(\frac{x}{w_x} \right)^2 + \left(\frac{y}{w_y} \right)^2 + \left(\frac{z'}{w_z} \right)^2 \right] \right\}, \quad (2)$$

where w_x , w_y and w_z are the pulse dimension along the x , y , and z' directions, respectively. Here the intensity distributions are assumed to be Gaussian in all three dimensions. The linear momentum density \mathbf{g} is the time average of the real part of $\varepsilon_0 (\mathbf{E} \times \mathbf{B})$ where \mathbf{E} is the electric field, \mathbf{B} is the magnetic field, and ε_0 is the permittivity in vacuum [2]. Following the Lorentz gauge, the linear momentum density \mathbf{g} is expressed in terms of the complex scalar function u [15]:

$$\mathbf{g} = \frac{\varepsilon_0}{2} (\mathbf{E}^* \times \mathbf{B} + \mathbf{E} \times \mathbf{B}^*) = \frac{\varepsilon_0}{2} \left(c \frac{\partial u^*}{\partial x} \frac{\partial u}{\partial z'} + c \frac{\partial u}{\partial x} \frac{\partial u^*}{\partial z'} + i\omega u \frac{\partial u^*}{\partial x} - i\omega u^* \frac{\partial u}{\partial x} \right) \mathbf{x} + \frac{\varepsilon_0}{2} \left(-i\omega u^* \frac{\partial u}{\partial y} + i\omega u \frac{\partial u^*}{\partial y} \right) \mathbf{y} + \frac{\varepsilon_0}{2} \left(-i\omega u^* \frac{\partial u}{\partial z'} + i\omega u \frac{\partial u^*}{\partial z'} + 2\omega k |u|^2 \right) \mathbf{z}' \quad (3)$$

where $*$ denotes complex conjugate, \mathbf{y} is the unit vector in the y direction, and \mathbf{z}' is the unit vector in the z' direction. The angular momentum density is given by the cross product of the position vector \mathbf{r} with the linear momentum density \mathbf{g} :

$$\begin{aligned}
\mathbf{r} \times \mathbf{g} = & \frac{\varepsilon_0}{2} \left[y \left(-i\omega u^* \frac{\partial u}{\partial z'} + i\omega u \frac{\partial u^*}{\partial z'} + 2\omega k |u|^2 \right) - z' \left(-i\omega u^* \frac{\partial u}{\partial y} + i\omega u \frac{\partial u^*}{\partial y} \right) \right] \mathbf{x} \\
& + \frac{\varepsilon_0}{2} \left[z' \left(c \frac{\partial u^*}{\partial x} \frac{\partial u}{\partial z'} + c \frac{\partial u}{\partial x} \frac{\partial u^*}{\partial z'} + i\omega u \frac{\partial u^*}{\partial x} - i\omega u^* \frac{\partial u}{\partial x} \right) - x \left(-i\omega u^* \frac{\partial u}{\partial z'} + i\omega u \frac{\partial u^*}{\partial z'} + 2\omega k |u|^2 \right) \right] \mathbf{y} \cdot (4) \\
& + \frac{\varepsilon_0}{2} \left[x \left(-i\omega u^* \frac{\partial u}{\partial y} + i\omega u \frac{\partial u^*}{\partial y} \right) - y \left(c \frac{\partial u^*}{\partial x} \frac{\partial u}{\partial z'} + c \frac{\partial u}{\partial x} \frac{\partial u^*}{\partial z'} + i\omega u \frac{\partial u^*}{\partial x} - i\omega u^* \frac{\partial u}{\partial x} \right) \right] \mathbf{z}'
\end{aligned}$$

The average OAM per photon within the wave packet can be derived through a volume integral:

$$OAM / photon = \frac{\int_{-\infty}^{\infty} \mathbf{r} \times \mathbf{g} dV}{\varepsilon_0 \omega^2 \int_{-\infty}^{\infty} |u|^2 dV} h\nu. \quad (5)$$

The average OAM per photon is a vector that has three components pointing to the x , y , and z' directions, respectively. Based on eqs. (2) to (5), the x , y , and z' components of the OAM per photon are derived analytically. For example, if $l_1 = 3$ and $l_2 = 2$, the x , y , and z' components of the OAM per photon are calculated to be 0 , $\frac{2(34w_x^2 + 7w_{z'}^2)}{41w_x w_{z'}} \hbar$, and $\frac{3(65w_x^2 + 17w_y^2)}{82w_x w_y} \hbar$,

respectively. Therefore, the OAM per photon within the wave packet is

$$\frac{1}{82} \sqrt{27506 + w_x^2 \left(\frac{38025}{w_y^2} + \frac{18496}{w_{z'}^2} \right) + \frac{2601w_y^2 + 784w_{z'}^2}{w_x^2}} \hbar \text{ pointing to the direction of } \theta \text{ degrees}$$

with respect to the $-y$ axis in the y - z' plane, where $\theta = \tan^{-1} \left(\frac{195w_x^2 w_{z'} + 51w_y^2 w_{z'}}{136w_x^2 w_y + 28w_y w_{z'}} \right)$. Particularly,

if w_x , w_y and $w_{z'}$ are of equal length, the x , y , and z' components of the OAM are 0 , $2\hbar$, and $3\hbar$ as expected. The theoretical analysis clarifies the fact that an average and three-dimensionally oriented OAM can indeed be obtained in a nonrelativistic way through the collision of a spatiotemporal vortex and a spatial vortex within one wave packet. The associated topological charges as well as the pulse dimensions play an important role in tuning the three-dimensional orientation of the tilted OAM.

3. Experimental demonstration

Experiments are designed and carried out to demonstrate the feasibility of achieving an ultrafast wave packet with a tilted OAM. The propagation characteristics of such a wave packet are also explored. As illustrated in fig. 1, a mode-locked fiber laser emits a chirped pulse of around 3 ps with a central wavelength of 1030 nm. A following pulse shaper that consists of a diffraction grating, a cylindrical lens and a two-dimensional spatial light modulator (SLM) applies a phase modulation in the spatial frequency - temporal frequency (k - ω) domain. After a two-dimensional spatiotemporal Fourier transform, phase vortices are retained in the spatiotemporal domain [11,12]. The topological charge of the spatiotemporal vortices can be adjusted through programming the phase pattern loaded on the SLM. The wave packet then acquires a spatial phase modulation with controllable topological charge from a following two-dimensional SLM. To characterize the field profile of the wave packet, a split pulse from the laser source is dechirped by a grating pair and utilized as a reference pulse. The reference pulse is shortened to around 90 fs. With the help of a precision linear stage, the reference pulse slices through the

chirped wave packet and obtains slices of interference fringe patterns for reconstructing the three-dimensional optical fields of the chirped wave packet [16,17].

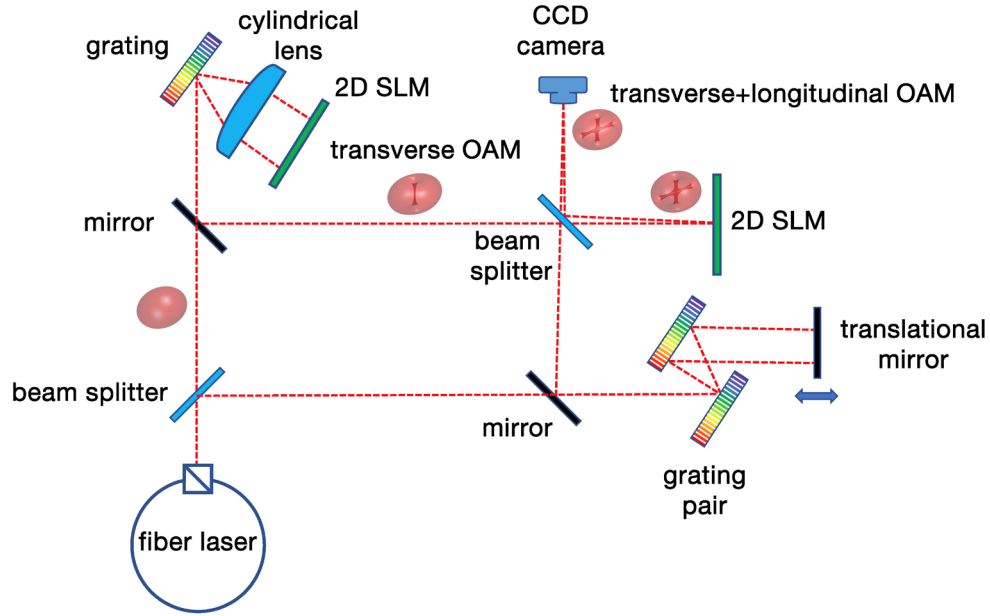


Fig. 1. Experimental setup to generate and characterize an ultrafast wave packet with a three-dimensionally oriented and time-varying OAM. The wave packet emitted from a mode-locked fiber laser acquires a spatiotemporal phase modulation through a pulse shaper and two-dimensional spatiotemporal Fourier transform. A spatial phase modulation is then applied to the wave packet by a second SLM.

Figure 2 shows the experimental data of the collision of a spatiotemporal vortex of topological charge 1 and a spatial vortex of topological charge 1. Figures 2a to 2d display four typical slices of interference images in the x - y plane of the chirped wave packet with the reference pulse. The positions of these slices are marked in fig. 2e. The fringe patterns in fig. 2a are dominantly influenced by the characteristics of a spatial vortex because the slicing position is far from the core of the spatiotemporal vortex. The most noticeable feature is a forklike pattern pointing downwards at the center that represents a spatial vortex of topological charge 1. As the reference pulse approaches the intersection center of the two orthogonal vortices, the feature of the spatiotemporal vortex becomes more obvious. In fig. 2b, the upper half of peripheral fringes starts to bend to the right indicating an increasing phase shift between the upper and lower part of the wave packet. Bending fringes is a salient feature of a spatiotemporal vortex. Continued in fig. 2c, the upper and lower peripheral fringes have a π phase difference. The dark fringes in the upper half are aligned with the bright fringes in the lower half. In fig. 2d, the bending direction of peripheral fringes is switched. Slicing through the chirped wave packet from head to tail, the upper and lower peripheral fringes complete a 0 to π and π to 0 phase shift. The peripheral areas of fringe patterns in figs. 2b to 2d have smaller spatial spiral phase gradient than the central areas. Therefore, the peripheral fringes mainly show the feature of a spatiotemporal vortex of topological charge 1. The central area of fig. 2b to 2d is the intersection of the spatiotemporal vortex line and the spatial vortex line. The interaction of the two vortices is most intense in the central region and the features of both vortices are combined.

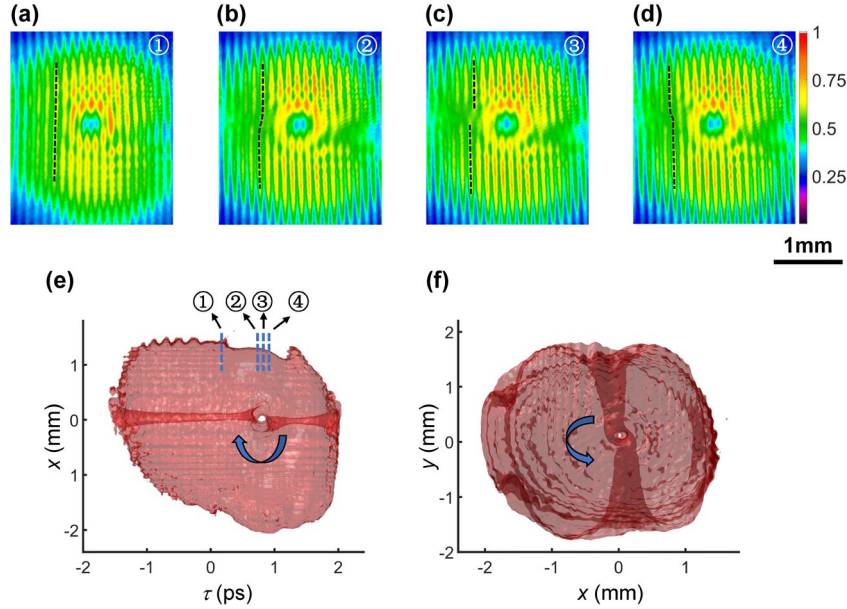


Fig. 2. The collision of a spatiotemporal vortex of topological charge 1 with a spatial vortex of topological charge 1. (a-d) Interference fringe patterns of the reference pulse with the chirped wave packet at various positions. **(e,f)** Three-dimensional intensity reconstruction of the chirped wave packet showing the intersection of a spatiotemporal vortex and a spatial vortex from different views. 91.0% energy of the wave packet is contained in the isosurface. The maximum intensity is normalized to 1 and the isovalue is 0.05.

Extracting the optical field information from slices of fringes, the three-dimensional intensity distributions of the wave packet can be reconstructed. Figures 2e and 2f show the wave packet from different views. Semitransparency is applied in order to see through the wave packet. In fig. 2e, a vortex core appearing as a tunnel resulted from spatiotemporal phase singularity is clearly displayed as a white circular area. The spatiotemporal vortex tunnel penetrates through the wave packet along the y direction. In fig. 2f, the spatial phase singularities result in a spatial vortex tunnel that penetrates all the way from head to tail of the wave packet. The spatiotemporal vortex tunnel (dark vertical strip in fig. 2f) is twisted counterclockwise at the core of the intersection of the two vortices. The spatial vortex tunnel (dark horizontal strip in fig. 2e), not surprisingly, is also twisted by the spatiotemporal vortex. The twisting phenomena are caused by diffraction of the wave packet propagating in free space. The spatial vortex diffracts in both x and y directions, however, the spatiotemporal vortex experiences diffraction effect only in x dimension. The imbalance of diffraction causes the twisting of the two vortex tunnels. Based on eq. (5), the OAM per photon of the wave packet is estimated to be $2.5\hbar$ pointing to the direction of 23.8 degrees with respect to the $-y$ axis in the y - z' plane. Numerical simulation results show that the OAM of the wave packet is conserved during free space propagation.

The second experimental demonstration shown in fig. 3 is the collision of two time-delayed spatiotemporal vortices of topological charge -1 and 1 with a spatial vortex of topological charge -1 in the same wave packet. Figures 3a to 3g are seven slices of interference fringe patterns from the positions marked in fig. 3h. Figures 3a to 3c show the interference patterns as the reference pulse slices through the intersection of the first spatiotemporal vortex with the spatial vortex. The upper half of peripheral fringes first bends to the left, then bends to the right after the π phase shift location. The first spatiotemporal vortex is therefore of topological charge -1 as also supported by the vortex tunnel twisting direction shown in fig. 3h. Figure 3d shows a slice between the two intersections where the spatial vortex plays a dominant role over the

spatiotemporal vortices. Consequently, the most noticeable feature is a forklike pattern pointing upwards at the center. Figures 3e to 3g display the interference patterns around the second intersection of orthogonal vortices. The second spatiotemporal vortex has a topological charge 1 that results in a different bending sequence shown in figs. 3e to 3g and an opposite twisting direction shown in fig. 3h. The average OAM of the wave packet in the head is estimated to be $3.4 \hbar$ pointing to the direction of 17.3 degrees with respect to the y axis in the y - z' plane; the average OAM of the wave packet in the tail is estimated to be to $6.2 \hbar$ pointing to the direction of 9.2 degrees with respect to the $-y$ axis in the y - z' plane. The self-torqued beams reported in Ref. [14] achieves the temporally non-static feature based on longitudinal OAM. In this work, the time-varying feature is built upon both transverse and longitudinal OAM. Consequently, besides the intriguing temporal feature, one more degree of freedom is added to the spatial feature of optical OAM. In this particular example, the OAM switching is temporally separated by around 1 ps. With shorter pulses, multiple OAM switching with temporal separation less than 100 fs packed in one wave packet can be expected.

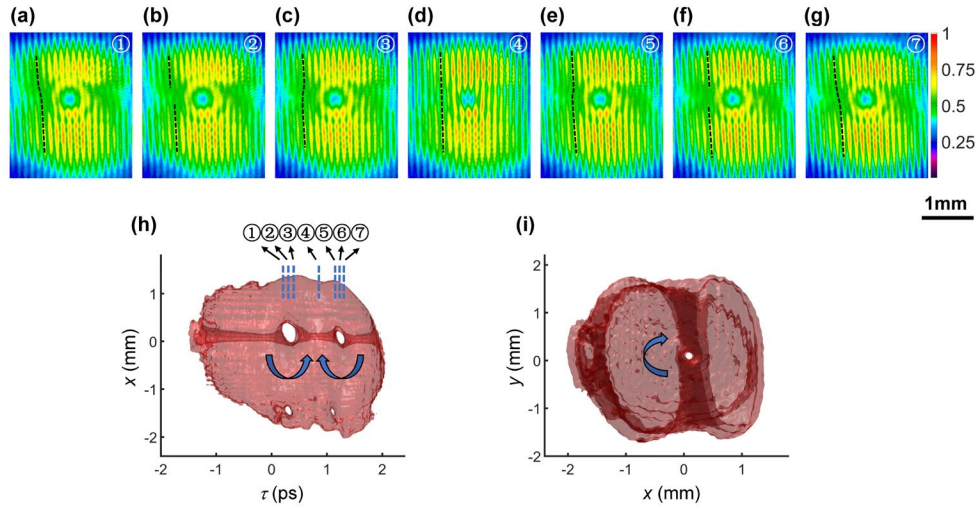


Fig. 3. The collision of two spatiotemporal vortices of topological charge -1 and 1 respectively with a spatial vortex of topological charge -1. (a-g) Interference fringe patterns of the reference pulse with the chirped wave packet at various positions. (h,i) Three-dimensional intensity reconstruction of the chirped wave packet showing the intersection of two spatiotemporal vortices and a spatial vortex from different views. 88.0% energy of the wave packet is contained in the isosurface. The maximum intensity is normalized to 1 and the isovalue is 0.05.

4. Conclusions

In summary, we report the theoretical and experimental demonstration of the generation of ultrafast wave packets carrying three-dimensionally oriented OAM and time-varying OAM with different orientations. The three-dimensional orientation of the OAM can be tuned by the topological charges of the spatiotemporal vortices and spatial vortices that collide within the packet as well as the pulse dimensions. Vortices with higher order topological charge can be incorporated by programming the phase information. The instability of higher order vortices propagating in free space or turbulent atmosphere may cause higher order vortices to break down into multiple unitary vortices. However, the OAM within the wave packet should be conserved. The extraordinary spatial and temporal features of optical OAM introduced in this work may find important applications in three-dimensional optical tweezing, spin-orbit angular momentum coupling, manipulating the OAM dichroism of nanostructures, or selectively exciting chiral quantum matter. This work will also stimulate further OAM research not only in optics and photonics, but also in many other fields that involves wave phenomena, including acoustics, electron beam, X-ray and so on.

Funding

National Natural Science Foundation of China (92050202, 61805142, 61875245); Shanghai Science and Technology Committee (19060502500); Shanghai Natural Science Foundation (20ZR1437600).

Author contribution

A. C. and C. W. proposed the original idea and performed all experiments and theoretical analysis. J. C. contributed in developing the measurement method. Q. Z. guided the theoretical analysis and supervised the project. All authors contributed to writing the manuscript.

Competing financial interest

The authors declare no competing financial interests.

Data availability

All data of this study are available from corresponding authors upon reasonable request.

Code availability

All codes used for data analysis and simulations are available from corresponding authors upon reasonable request.

References

1. G. Gbur, *Singular Optics* (CRC Press, Florida, 2016).
2. L. Allen, M. Beijersbergen, R. Spreeuw, and J. Woerdman, "Orbital angular momentum of light and the transformation of Laguerre–Gaussian laser modes," *Phys. Rev. A* **45**, 8185-8189 (1992).
3. V. Pasko, M. Soskin, and M. Vasnetsov, "Transversal optical vortex," *Opt. Commun.* **198**(1), 49-56 (2001).
4. A. Bekshaev, M. Vasnetsov, V. Denisenko, and M. Soskin, "Transformation of the orbital angular momentum of a beam with optical vortex in an astigmatic optical system," *JETP Lett.* **75**(3), 127-130 (2002).
5. G. Molinaterri, J. Recolons, J. Torres, L. Torner, and E. Wright, "Observation of the dynamical inversion of the topological charge of an optical vortex," *Phys. Rev. Lett.* **87**(2) 023902 (2001).
6. J. Wang, J. Yang, I. Fazal, N. Ahmed, Y. Yan, H. Huang, Y. Ren, Y. Yue, S. Dolinar, M. Tur, and A. Willner, "Terabit free-space data transmission employing orbital angular momentum multiplexing," *Nat. Photon.* **6** 488-496 (2012).
7. A. Willner, H. Huang, Y. Yan, Y. Ren, N. Ahmed, G. Xie, C. Bao, L. Li, Y. Cao, Z. Zhao, J. Wang, M. Lavery, M. Tur, S. Ramachandran, A. Molisch, N. Ashrafi, and S. Ashrafi, "Optical communications using orbital angular momentum beams," *Adv. Opt. Photon.* **7**, 66-106 (2015).
8. C. Maurer, A. Jesacher, S. Bernet, M. Ritsch-Marte, "What spatial light modulators can do for optical microscopy," *Laser & Photon. Rev.* **5**, 81-101 (2011).
9. J. Courtial and M. Padgett, "Limit to the orbital angular momentum per unit energy in a light beam that can be focussed onto a small particle," *Opt. Commun.* **173**, 269-274 (2000).
10. A. Mair, A. Vaziri, G. Weihs, and A. Zeilinger, "Entanglement of the orbital angular momentum states of photons," *Nature* **412**, 313-316 (2001).
11. S. Hancock, S. Zahedpour, A. Goffin, and H. Milchberg, "Free-space propagation of spatiotemporal optical vortices," *Optica* **6**, 1547-1553 (2019).
12. A. Chong, C. Wan, J. Chen, and Q. Zhan, "Generation of spatiotemporal optical vortices with controllable transverse orbital angular momentum," *Nat. Photon.* **14**, 350-354 (2020).
13. K. Bliokh, and F. Nori, "Spatiotemporal vortex beams and angular momentum," *Phys. Rev. A* **86**, 033824 (2012).
14. L. Rego, K. Dorney, N. Brooks, Q. Nguyen, C. Liao, J. Roman, D. Couch, A. Liu, E. Pisanty, M. Lewenstein, L. Plaja, H. Kapteyn, M. Murnane, and C. Hernandez-Garcia, "Generation of extreme-ultraviolet beams with time-varying orbital angular momentum," *Science* **364**(6447): eaaw9486 (2019).
15. A. Lotti, A. Couairon, D. Faccio, and P. Trapani, "Energy-flux characterization of conical and space-time coupled wave packets," *Phys. Rev. A*, **81**(2), 023810 (2010).
16. Y. Li and J. Lewellen, "Generating a quasiellipsoidal electron beam by 3D laser-pulse shaping," *Phys. Rev. Lett.* **100**, 074801 (2008).
17. H. Li, I. Bazarov, B. Dunham, and F. Wise, "Three-dimensional laser pulse intensity diagnostic for photoinjectors," *Phys. Rev. ST Accel. Beams* **14**, 112802 (2011).